

WASP-3b: a strongly-irradiated transiting gas-giant planet

D. Pollacco^{1*}, I. Skillen⁷, A. Collier Cameron², B. Loeillet¹¹, H.C. Stempels²,
F. Bouchy^{12,13}, N.P. Gibson¹, L. Hebb², G. Hébrard¹², Y.C. Joshi¹, I. McDonald⁵,
B. Smalley⁵, A.M.S. Smith², R.A. Street^{1,15}, S. Udry¹⁰, R.G. West³, D.M. Wilson⁵,
P.J. Wheatley⁹, S. Aigrain⁶, C.R. Benn⁷, V.A. Bruce², D.J. Christian¹, W.I. Clarkson^{4,14},
B. Enoch⁴, A. Evans⁵, A. Fitzsimmons¹, C.A. Haswell⁴, C. Hellier⁵, S. Hickey^{7,16},
S.T. Hodgkin⁶, K. Horne², M. Hrudková^{7,17}, J. Irwin⁶, S.R. Kane⁷, F.P. Keenan¹,
T.A. Lister^{2,5,15}, P. Maxted⁵, M. Mayor¹⁰, C. Moutou¹¹, A.J. Norton⁴, J. P. Osborne³,
N. Parley⁴, F. Pont¹⁰, D. Queloz¹⁰, R. Ryans¹, and E. Simpson¹

¹*Astrophysics Research Centre, School of Mathematics & Physics, Queen's University, University Road, Belfast, BT7 1NN, UK*

²*School of Physics and Astronomy, University of St Andrews, North Haugh, St Andrews, Fife KY16 9SS, UK*

³*Department of Physics and Astronomy, University of Leicester, Leicester, LE1 7RH, UK*

⁴*Department of Physics and Astronomy, The Open University, Milton Keynes, MK7 6AA, UK*

⁵*Astrophysics Group, Keele University, Staffordshire, ST5 5BG*

⁶*Institute of Astronomy, University of Cambridge, Madingley Road, Cambridge, CB3 0HA, UK*

⁷*Isaac Newton Group of Telescopes, Apartado de Correos 321, E-38700 Santa Cruz de la Palma, Tenerife, Spain*

⁸*Department of Astronomy, University of Florida, 211 Bryant Space Science Center, Gainesville, FL 32611-2055, USA*

⁹*Department of Physics, University of Warwick, Coventry CV4 7AL, UK*

¹⁰*Observatoire de Genève, Université de Genève, 51 Ch. des Maillettes, 1290 Sauverny, Switzerland*

¹¹*Laboratoire d'Astrophysique de Marseille, BP 8, 13376 Marseille Cedex 12, France*

¹²*Institut d'Astrophysique de Paris, CNRS (UMR 7095) – Université Pierre & Marie Curie, 98^{bis} bd. Arago, 75014 Paris, France*

¹³*Observatoire de Haute-Provence, 04870 St Michel l'Observatoire, France*

¹⁴*STScI, 3700 San Martin Drive, Baltimore, MD 21218, USA*

¹⁵*Las Cumbres Observatory, 6740 Cortona Dr. Suite 102, Santa Barbara, CA 93117, USA*

¹⁶*Centre for Astrophysics, Science & Technology Research Institute, University of Hertfordshire, Hatfield, AL10 9AB, UK*

¹⁷*Astronomical Institute, Charles University Prague, V Holesovickach 2, CZ-180 00 Praha, Czech Republic*

Accepted 1988 December 15. Received 1988 December 14; in original form 1988 October 11

ABSTRACT

We report the discovery of WASP-3b, the third transiting exoplanet to be discovered by the WASP and SOPHIE collaboration. WASP-3b transits its host star USNO-B1.0 1256-0285133 every 1.846834 ± 0.000002 days. Our high precision radial-velocity measurements present a variation with amplitude characteristic of a planetary-mass companion and in-phase with the light-curve. Adaptive optics imaging shows no evidence for nearby stellar companions, and line-bisector analysis excludes faint, unresolved binarity and stellar activity as the cause of the radial-velocity variations. We make a preliminary spectroscopic analysis of the host star finding it to have $T_{\text{eff}} = 6400 \pm 100 \text{ K}$ and $\log g = 4.25 \pm 0.05$ which suggests it is most likely an unevolved main sequence star of spectral type F7–8V. Our simultaneous modelling of the transit photometry and reflex motion of the host leads us to derive a mass of $1.76^{+0.08}_{-0.14} M_J$ and radius $1.31^{+0.07}_{-0.14} R_J$ for WASP-3b. The proximity and relative temperature of the host star suggests that WASP-3b is one of the hottest exoplanets known, and thus has the potential to place stringent constraints on exoplanet atmospheric models.

Key words: methods: data analysis – stars: planetary systems – techniques: radial velocities – techniques: photometric

1 INTRODUCTION

Since the discovery by Henry et al. (2000) and Charbonneau et al. (2000) of the first exoplanet found to transit its host star, HD209458b, a further 22 transiting systems have been announced (see <http://obswww.unige.ch/~pont/TRANSITS.htm>). Transiting exoplanets are highly prized because the transit geometry constrains the orbital inclination, and this in turn allows their masses and radii to be determined directly. The mass-radius relation for exoplanets allows us to probe their internal structure, since it is these parameters which are compared with models of planetary structure and evolution (Sato et al. 2005; Guillot 2006). The limited numbers of transiting exoplanets studied so far show remarkable diversity in their physical parameters. For example, planets with masses $M \sim 1M_J$ range in size from $0.8\text{--}1.5R_J$ for reasons that still elude us, although several plausible explanations have been proposed (eg Arras & Bildsten 2006; Burrows et al. 2007; Fortney et al. 2007; Gu et al. 2004). The discovery of transiting planets in greater numbers will allow us to further explore the mass-radius plane, and thereby constrain theories of planetary formation, migration and evolution.

The discovery of the first exoplanet, 51 Peg b, was by the radial-velocity method (Mayor & Queloz 1995), and this technique is responsible for the discovery of the vast majority of the known exoplanetary systems, including HD209458b. However, following the discovery of the transits of HD209458b (Henry et al. 2000; Charbonneau et al. 2000) it was widely believed that the multiplex advantage of wide-field photometric imaging could lead to this technique becoming the dominant method for detecting exoplanets. While it is true to say that, at least initially, photometric surveys have been slow to realise their expected detection rates (Horne 2003), recently this situation has begun to change with 14 new systems published in 2006-07 alone. This improved detection rate is largely due to the development of a better understanding of noise characteristics, especially the correlated noise inherent in such photometric surveys (Pont et al. 2006). Transiting planets now comprise approximately 10% of the known exoplanets. Successful exoplanet photometric surveys include Wide Angle Search for Planets (WASP) Project (Pollacco et al. 2006), the Hungarian Automatic Telescope (HAT) Network (Bakos et al. 2004), OGLE (Udalski et al. 2002), the Transatlantic Exoplanet (TrES) Survey (Dunham et al. 2004; O'Donovan et al. 2006) and the XO group (McCullough et al. 2006). The WASP project has published two new systems in the last year WASP-1b and WASP-2b (Collier Cameron et al. 2007a) and WASP-1b, in particular, has proved to be especially interesting, being well oversized compared to other planets for its mass.

In this paper the WASP and SOPHIE collaboration announce the discovery of a new, relatively high mass, strongly-irradiated gas-giant exoplanet, WASP-3b.

2 OBSERVATIONS AND DATA REDUCTION

2.1 SuperWASP-N Photometry

The photometric observations used in this study are from the inaugural 2004 SuperWASP-N observing season, which

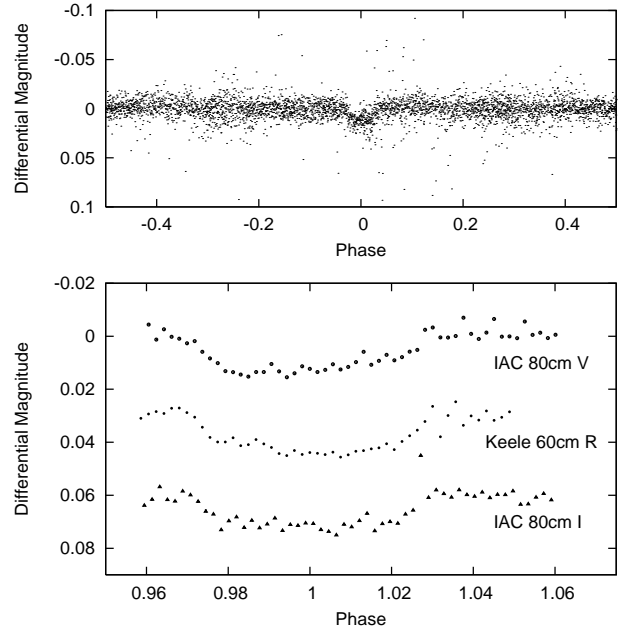


Figure 1. Light Curves for 1SWASP J183431.62+353941.4 (WASP-3) obtained with SuperWASP-N (top panel), the IAC 80-cm telescope (V and I) and the Keele 60-cm telescope (R) as marked. All the data (apart from that from SuperWASP-N) was averaged in 300 second bins. The data was phased using the ephemeris derived in Section 3.2.1, $T_0 = 2454143.8504$ and $P = 1.846834$ days.

ran from April to September of that year; this data set also led to the discovery of WASP-1b and WASP-2b. Briefly, in 2004 the SuperWASP-N instrument comprised 4, and at times, 5 optical cameras, each consisting of a Canon 200 mm f/1.8 telephoto lens imaging onto a thermoelectrically-cooled, science-grade 2048×2048 CCD camera (manufactured by e2v Technologies PLC). In this system, the CCD's $13.5 \mu\text{m}$ pixels project to an angular size of 14.2 arcseconds. For the entirety of the 2004 season, while robotic operation was being commissioned, the instrument performance was supervised with an observer always in attendance, although data acquisition was fully automated. Data were shipped to the UK on a weekly basis and reduced at the home institutes of the WASP Consortium using a dedicated, purpose-built pipeline, and the results ingested into the project database at the University of Leicester. The entire project infrastructure is described in detail by Pollacco et al. (2006) along with the deployment of a further facility, WASP-S, at the South African Astronomical Observatory. SuperWASP-N now runs completely robotically, and data are transferred to the UK in near real-time over the Internet.

Transit searches were carried out on this dataset (Christian et al. 2006; Clarkson et al. 2007; Lister et al. 2007; Street et al. 2007) using the techniques outlined by Collier Cameron et al. (2006). 1SWASP J183431.62+353941.4, which we henceforth denote as WASP-3, was highlighted by Street et al. (2007) as a high-priority candidate worthy of further study. Figure 1 (top panel) shows the original SuperWASP-N lightcurve, which comprises 3969 data points obtained over a 118 day period.

In the original SuperWASP-N photometry 17 transits were observed with >50% of a transit observed on 10 occasions. These data led to an ephemeris of $T_0=2453139.1748$ and $P=1.846800$ which was used to arrange followup observations. The transit here has a depth of 0.013 mag. and is 137 minutes in duration.

2.2 Higher precision photometric observations

WASP-3 was observed with the IAC 80 cm telescope as part of the Canarian Observatories' *International Time Programme* for 2007. The imaging camera on this telescope has an e2v Technology PLC CCD of 2148×2148 pixels giving a scale of 0.33 arcseconds/pixel and a total field of view of 10.6 arcminutes. Observations were taken during the transit of 2007 August 4, and consist of 327 images of 30 and 20 seconds integration in the V and I bands respectively. This night was photometric but suffered from significant Saharan dust extinction, estimated to be ~ 0.4 mag on La Palma from the SuperWASP-N real-time pipeline.

The images were bias subtracted with a stacked bias frame and flat-fielded with a stacked twilight flat field image obtained in both filters using individual flats gathered over the course of the run. After the instrumental signatures were removed, source detection and aperture photometry were performed on all science frames using the CASU catalogue extraction software (Irwin & Lewis 2001). We chose an aperture size matched to the typical seeing (5 pixels, $1.5''$) and selected 5 non-variable comparison stars in the field of WASP-3 to use in deriving the differential photometry. For each exposure, we summed the fluxes of the 5 comparison stars and divided by the flux of the target star to derive the differential magnitude of the target. The resulting V and I band lightcurves (Figure 1) of WASP-3 have a precision of ~ 4 millimag.

Further observations of WASP-3 were made with the Keele University Observatory 60cm Thornton Reflector on 2007 September 10. This telescope is equipped with a 765×510 pixel Santa Barbara Instrument Group (SBIG) ST7 CCD at the $f/4.5$ Newtonian focus, giving a 0.68 arcsecond/pixel resolution and a 8.63×5.75 arcminute field of view. During most of the period the weather was photometric except post egress where some cloud appeared. Altogether 644×20 sec observations in the R band were obtained. After applying corrections for bias, dark current and flat fielding in the usual way, aperture photometry on two comparisons were performed using the commercial software AIP4Win (Berry & Burnell 2005).

Tracking errors and spurious electronic noise mean that systematic noise is introduced into the system at an estimated level of 2 millimag with periodicities of 2 and ~ 20 minutes. No corrections have been applied for this effect.

2.3 OHP 1.9 m and SOPHIE

WASP-3 was observed with the Observatoire de Haute-Provence's 1.93 m telescope and the SOPHIE spectrograph (Bouchy et al. 2006), over the 8 nights 2007 July 2 – 5 and August 27 – 30; a total of 7 usable spectra were acquired. SOPHIE is an environmentally stabilized spectrograph designed to give long-term stability at the level of a few m s^{-1} .

We used the instrument in its high efficiency mode, acquiring simultaneous star and sky spectra through separate fibres with a resolution of $R=40000$. Thorium-Argon calibration images were taken at the start and end of each night, and at 2- to 3-hourly intervals throughout the night. The radial-velocity drift never exceeded 2-3 m/s, even on a night-to-night basis.

Conditions during both runs varied from photometric to cloudy, but all nights were affected by strong moonlight. As WASP-3 has magnitude $V \sim 10.5$, integrations of 900 sec give a peak signal-to-noise per resolution element of around 40-50. The 2MASS colours and reduced proper motion for WASP-3 suggest a spectral type of about F7-8V, hence we cross-correlated the spectra against a G2V template provided by the SOPHIE control and reduction software.

In all spectra the cross-correlation functions (CCF) were contaminated by the strong moonlight. We corrected them by using the CCF from the background light's spectrum (mostly the Moon) in the sky fibre. We then scaled both CCFs using the difference of efficiency between the two fibres. Finally we subtracted the corresponding CCF of the background light from the star fibre, and fitted the resulting function by a Gaussian. The parameters obtained allow us to compute the photon-noise uncertainty of the corrected radial velocity measurement (σ_{RV}), using the relation detailed in Collier Cameron et al. (2007a):

$$\sigma_{RV} = 1.7 * \sqrt{(FWHM)/(SNR * Contrast)}$$

Overall our RV measurements have an average photon-noise uncertainty of 14 m/s. As our radial velocity measurements are not photon-noise limited, we quadratically added a radial velocity component to those uncertainties of about 10 m/s (more details in Section 3.2.1). The log of the observations and barycentric RV is given in Table 1.

3 RESULTS AND ANALYSES

3.1 Stellar parameters

The SOPHIE spectra are individually of modest signal-to-noise, but when summed together they are suitable for a preliminary photospheric analysis of WASP-3. However, from experience we have found that the SOPHIE standard pipeline reduction does not fully remove the scattered light component within the spectrograph. While this does not affect radial velocities significantly, it can nonetheless have subtle effects on absorption line depths, adversely affecting the derived spectral synthesis parameters. Therefore we carefully re-reduced the first three raw images taken over 2–5 July 2007 with the REDUCE echelle data reduction package (Piskunov & Valenti 2002), paying careful attention to the issue of scattered light. These data are least affected by moonlight.

Following our analysis of WASP-1 (Stempels et al. 2007), we employed the methodology of Valenti & Fischer (2005), using the same tools, techniques and model atmosphere grid. We used the IDL-based software *Spectroscopy Made Easy* (SME) (Valenti & Piskunov 1996) to calculate and fit synthetic spectra using a multi-dimensional least squares approach.

We concentrated our analysis on five regions in the spectrum (see Figure 2). These regions allow us to constrain the

Table 1. Journal of radial-velocity measurements of WASP-3. The 1SWASP identifiers give the J2000 stellar coordinates of the photometric apertures; the USNO-B1.0 number denotes the star for which the radial-velocity measurements were secured. The quoted uncertainties in the radial velocity errors include components due to photon noise (Section 2.3) and 10m/s of jitter (Section 3.2.1) added in quadrature. The fourth and fifth columns give the FWHM of the CCF dip and the contrast of the dip as a fraction of the weighted mean continuum level. The signal-to-noise ratio at 550nm is given in column six.

BJD	t_{exp} (s)	V_r km s ⁻¹	FWHM km s ⁻¹	Contrast %	S:N	Notes
1SWASP J183431.62+353941.4: USNO-B1.0 1256-0285133 = GSC 02636-00195 = WASP-3						
2454286.5225	900	-5.751 ± 0.018	20.5	11.7	44	Photometric
2454287.4563	900	-5.254 ± 0.020	19.8	11.8	37	Cloud and Moonlight
2454289.3662	900	-5.259 ± 0.018	19.9	11.8	43	Photometric and Moonlight
2454340.3251	1800	-5.648 ± 0.013	19.7	12.2	75	Moonlight
2454341.3989	900	-5.406 ± 0.015	19.7	12.1	53	Moonlight
2454342.3198	900	-5.544 ± 0.019	19.8	12.0	39	Cloud and Moonlight
2454343.4825	2100	-5.638 ± 0.013	19.8	12.2	75	Cloud and Moonlight

Table 2. Parameters for WASP-3 as derived from the SME analysis of the SOPHIE spectroscopy.

Parameter	WASP-3
T_{eff}	6400 ± 100 K
$\log g$	4.25 ± 0.05
[M/H]	0.00 ± 0.20
$v \sin i$	13.4 ± 1.5 km/s
v_{rad}	-5.490 km/s

stellar effective temperature, T_{eff} , (through the broad wings of H α and, to a lesser extent, Na I D 5890Å), gravity, $\log g$, (through Mg I b 5175Å and Na I D 5890Å) and the metallicity, [M/H], (through the weak photospheric absorption lines in the 6000–6200Å region). We also measured the abundance of lithium from the Li I 6708Å line. The combined spectrum is not of sufficient quality to perform a detailed abundance analysis. The parameters we obtained from this analysis are listed in Table 2, and a comparison between observed and synthesized profiles is shown in Figure 2. In addition to the spectrum analysis, we also used Tycho B and V , and 2MASS photometry to estimate the effective temperature using the Infrared Flux Method (Blackwell & Shallis 1977). This gives $T_{\text{eff}} = 6200 \pm 300$ K, which is in close agreement with that obtained from the spectroscopic analysis. The Tycho and 2MASS colours ($V - K = 1.32$, $V - H = 0.2$) also suggest a spectral type of F7–8V (Street et al. 2007; Collier Cameron et al. 2006).

In our spectra the Li I λ 6708Å line is weak, but still measurable, and we derive a Lithium abundance of $\log n(\text{Li}) + 12 = 2.0 - 2.5$. However, at this stellar temperature it is thought that stellar age does not correlate well with Lithium abundance (Sestito & Randich 2005), so we have examined the evolutionary tracks for low and intermediate-mass stars presented by Girardi et al. (2000) using a maximum-likelihood fitting routine. Using our derived stellar parame-

ters we find the stellar mass $M_* = 1.24 \pm 0.08$ with an age of 0.7 – 3.5 Gyr.

3.2 The reflex motion of the host star

3.2.1 Markov-chain Monte Carlo analysis

The SOPHIE radial-velocity data measurements are plotted in Figure 3 together with the best-fitting global fit to the SuperWASP-N, IAC80 and Keele transit photometry. Since the timing of the transits and the radial-velocity solution both provide information about the orbit, we modelled the transit photometry and the reflex motion of the host star simultaneously.

The model of the primary star’s radial-velocity orbit is parametrised in the usual way by the primary’s radial-velocity amplitude K_1 , the centre-of-mass velocity γ , the orbital eccentricity e and the longitude ω of periastron.

The transit profile was modelled using the small-planet approximation of Mandel & Agol (2002), with the 4-coefficient nonlinear limb-darkening model of Claret (2000). We used R -band limb-darkening coefficients for the SuperWASP-N data, whose unfiltered wavelength response is centred near the R band, and for the Keele R -band data. We used the appropriate V and I -band limb-darkening coefficients for the IAC80 photometry. The transit model was characterised by the epoch T_0 of mid-transit, the orbital period P , the duration t_T from first to fourth contact, the squared ratio $\Delta F = (R_p/R_*)^2$ of the planet radius R_p to the stellar radius R_* , and the impact parameter $b = a(1 - e \cos E_T) \cos i / R_*$ of the planet’s trajectory across the face of the host star. Here a is the orbital semi-major axis, E_T is the eccentric anomaly at the epoch of transit and i is the orbital inclination. The ratio of the stellar radius to the orbital separation is then given approximately (or exactly for a circular orbit) by

$$\frac{R_*}{a} = \frac{t_T}{P} \frac{\pi}{(1 + \sqrt{\Delta F})^2 - b^2}$$

(Collier Cameron et al. 2007b). The orbital semi-major axis is derived from the orbital period and the stellar mass M_*

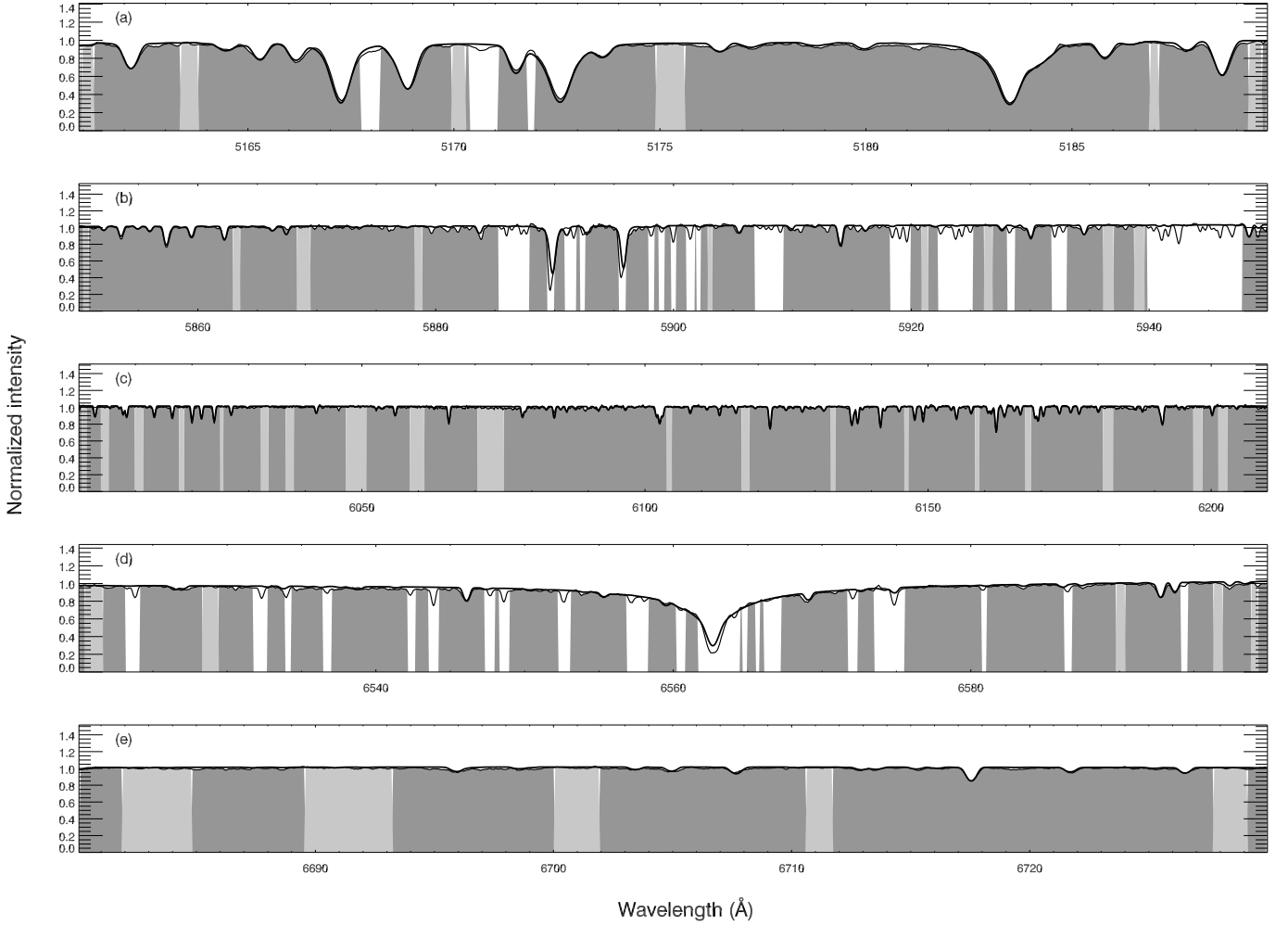


Figure 2. A comparison between the observed SOPHIE spectrum of WASP-3 and the calculated spectrum obtained from spectral synthesis with SME, using the atmospheric parameters from Table 2. The white regions are excluded from the spectral analysis, mainly because of the presence of telluric absorption. Light shaded regions were used to determine the continuum level, and the remaining dark shaded regions to determine the stellar atmospheric parameters. All five spectral sections were used simultaneously. The five sections contain (a) the Mg I b triplet at 5175Å (b) the Na I D doublet at 5890Å/ (c) a large region with well-isolated lines of a wide range of metals (d) the H α line at 6563Å/ and (e) the Li I line at 6707Å.

via Kepler's third law. The stellar mass is estimated from the $J-H$ colour as described by Collier Cameron et al. (2007b).

The set of nine parameters $\{T_0, P, t_T, \Delta F, b, M_*, K_1, e, \omega\}$ thus defines both the transit light curve and the form of the reflex velocity variation. We compute the photometric zero-point offset Δm of the observed magnitudes m_j from the model μ_j derived from a given set of parameters:

$$\Delta m = \frac{\sum_j (m_j - \mu_j) w_j}{\sum_j w_j}.$$

The weights w_j are the inverse variances $1/\sigma_j^2$ of the individual observations. Similarly, we compute the radial velocity γ of the system's centre of mass as the inverse-variance weighted mean offset between the observed radial velocities v_k and the model values ν_k for the current model param-

eters:

$$\gamma = \frac{\sum_k (v_k - \nu_k) w_k}{\sum_k w_k}.$$

We quantify the goodness of fit to the data by the combined χ^2 statistic for the combined photometric and radial-velocity data:

$$\chi^2 = \sum_{j=1}^{N_p} \frac{(m_j - \mu_j - \Delta m)^2}{\sigma_j^2} + \sum_{k=1}^{N_v} \frac{(v_k - \nu_k - \gamma)^2}{\sigma_k^2}.$$

Markov-Chain Monte-Carlo analysis has recently become established as an efficient and reliable method for establishing both photometric (Holman et al. 2006; Burke et al. 2007) and orbital (Ford 2006; Gregory 2007) parameters of close-orbiting giant exoplanets. We determined the photometric and orbital parameters of the WASP-3 system using the Markov-chain Monte-Carlo algorithm described in detail by Collier Cameron et al. (2007b), to which

Table 3. WASP-3 system parameters and 1- σ error limits derived from MCMC analysis.

Parameter	Symbol	Value	Units
Transit epoch (BJD)	T_0	$2454143.8503^{+0.0004}_{-0.0003}$	days
Orbital period	P	$1.846834^{+0.000002}_{-0.000002}$	days
Planet/star area ratio	$(R_p/R_s)^2$	$0.0106^{+0.0002}_{-0.0004}$	
Transit duration	t_T	$0.1110^{+0.0009}_{-0.0018}$	days
Impact parameter	b	$0.505^{+0.051}_{-0.166}$	R_*
Stellar reflex velocity	K_1	$0.2512^{+0.0079}_{-0.0108}$	km s $^{-1}$
Centre-of-mass velocity	γ	$-5.4887^{+0.0013}_{-0.0018}$	km s $^{-1}$
Orbital semimajor axis	a	$0.0317^{+0.0005}_{-0.0010}$	AU
Orbital inclination	I	$84.4^{+2.1}_{-0.8}$	degrees
Stellar mass	M_*	$1.24^{+0.06}_{-0.11}$	M_\odot
Stellar radius	R_*	$1.31^{+0.05}_{-0.12}$	R_\odot
Stellar surface gravity	$\log g_*$	$4.30^{+0.07}_{-0.03}$	[cgs]
Stellar density	ρ_*	$0.55^{+0.15}_{-0.05}$	ρ_\odot
Planet radius	R_p	$1.31^{+0.07}_{-0.14}$	R_J
Planet mass	M_p	$1.76^{+0.08}_{-0.14}$	M_J
Planetary surface gravity	$\log g_p$	$3.37^{+0.09}_{-0.04}$	[cgs]
Planet density	ρ_p	$0.78^{+0.28}_{-0.09}$	ρ_J
Planet temp ($A = 0$)	T_{eq}	1960^{+33}_{-76}	K

we refer the reader for most details of the implementation. The initial photometric solution for the SuperWASP-N transit profiles is established by our transit-search algorithm (Collier Cameron et al. 2006). The initial radial-velocity solution is an inverse variance-weighted linear least-squares fit assuming a circular orbit. In both cases, the initial fits also yield good estimates of the parameter uncertainties. The stellar mass is initialised at the value M_0 estimated from the $J - H$ colour.

At each step in the algorithm, each of the nine proposal parameters is perturbed by a small random amount such that

$$T_{0,i} = T_{0,i-1} + \sigma_{T_0} G(0, 1)f$$

and similarly for the other eight parameters. Here $G(0, 1)$ is a random Gaussian deviate with mean zero and unit standard deviation. The adaptive step-size controller f is initially set to 0.5, and evolves as the calculation progresses, ensuring that roughly 25 percent of proposal sets are accepted.

The prior probability distributions for all nine parameters are treated as being uniform. The parameters P , t_T , ΔF , M_* and K_1 are required to be positive. The impact parameter and eccentricity are restricted to the ranges $0 < b < 1$ and $0 < e < 1$, while the longitude of periastron is restricted to the range $-\pi < \omega < \pi$. The decision on whether or not to accept a set of proposal parameters is made via the Metropolis-Hastings algorithm using the logarithmic likelihood functional

$$Q_i = \chi_i^2 + \frac{(M_{*,i} - M_0)^2}{\sigma_M^2} + \frac{(\log g_{*,i} - \log g_*)^2}{\sigma_{\log g}^2},$$

where $\log g_{*,i}$ is computed directly from the mass $M_{*,i}$ and radius $R_{*,i}$. This imposes a Gaussian prior on the stellar

mass, and indirectly on the radius. The prior forces the stellar mass to be close to the initial estimate M_0 with an assumed uncertainty $\sigma_M = 0.1M_0$. The prior on $\log g_*$ ensures consistency with the spectroscopically-measured value $\log g_* = 4.25 \pm 0.05$, and thus helps to reduce the uncertainty in the stellar radius if the impact parameter is not strongly constrained by the photometry.

If a new set of proposal parameters yields $Q_i < Q_{i-1}$, the fit to the data is improved and the proposal is accepted. If $Q_i > Q_{i-1}$, the parameter set is accepted with probability $\exp[(Q_{i-1} - Q_i)/2]$. We find that the solution converges within a few hundred steps to a stable, optimal solution. After this initial "burn-in" phase, we re-scale the photometric error bars so that the contribution of each photometric dataset to χ^2 is equal to the associated number of degrees of freedom. For the radial velocity data, we estimate the additional variance needed to match their contribution to χ^2 with the number of degrees of freedom. This is equivalent to adding radial-velocity "jitter" with amplitude 10 m s $^{-1}$ in quadrature with the photon noise uncertainties giving the values listed in Table 1. We then run the algorithm for a few hundred further steps and derive revised parameter uncertainties from the standard deviations of their respective Markov chains. This optimises the step length used in generating new sets of proposal parameters. Finally the algorithm is allowed to run for 10^5 steps in order to map out the joint posterior probability distribution of the nine proposal parameters.

We find that for WASP-3 the nine proposal parameters show only weak mutual correlations. The correlation lengths (Tegmark et al. 2004) of the Markov chains for individual parameters are typically 10 to 20 steps, so the final production run yielded approximately 10^4 statistically

Table 4. Dependence of stellar and planetary parameters on $\log g_*$.

$\log g$ (cgs)	χ^2_{ph}	b	M_* (M_\odot)	R_* (R_\odot)	R_p (R_J)	ρ_p (ρ_J)
4.05	4492.6	0.76	1.14	1.64	1.75	0.31
4.15	4478.6	0.68	1.18	1.50	1.55	0.46
4.25	4470.9	0.58	1.23	1.37	1.39	0.65
4.35	4468.1	0.38	1.22	1.22	1.20	1.00
4.45	4468.9	< 0.09	1.36	1.17	1.14	1.25
4.55	4491.1	< 0.05	1.60	1.20	1.16	1.32

independent parameter sets. In the initial runs we allowed all nine parameters to float, and arrived at a solution with eccentricity $e = 0.05 \pm 0.05$. Since this is statistically indistinguishable from the circular orbit expected for a planet with such a short period, the remaining eight parameters were fitted assuming $e = 0$.

The values of the parameters at the optimal solution are given, together with their associated $1-\sigma$ (68.3 percent) confidence intervals, in Table 3. These results are consistent with those derived from the spectral analysis presented earlier.

We explored the relationship between the stellar surface gravity and the impact parameter of the transit by repeating the fit for a sequence of values of $\log g$, with an artificially restricted $\sigma_{\log g} = 0.01$. The results are given in Table 4. The best formal fit to the photometry is obtained for stellar surface gravities in the range $4.35 < \log g < 4.45$. In this range, however, the stellar radius is unphysically low in relation to the stellar mass. At the spectroscopically-determined $\log g = 4.25$, the photometric χ^2 is only marginally degraded. At still lower values of $\log g$, the impact parameter increases to the point where the duration of transit ingress and egress cannot be fitted satisfactorily. Moreover, the radii of the star and the planet become implausibly inflated. We conclude that the stellar surface gravity must lie in the range $4.25 < \log g < 4.35$, and the impact parameter in the range $0.4 < b < 0.6$. The limits on these parameters derived from the full posterior probability distribution, as listed in Table 3, are consistent with this conclusion.

3.2.2 Line-bisector analysis

It is well known that faint binaries contaminating the photometric aperture, or even stellar activity, can influence absorption line shape and can, in certain circumstances, mimic or confuse small radial velocity motions. By noting the position of the line-bisector of the cross-correlation function, asymmetries in the profile will become apparent.

We measured the asymmetries of the cross-correlation function peaks using the line-bisector method as a function of radial velocity (Gray 1988), as applied by Queloz et al. (2001). Figure 4 demonstrates that periodic variations, indicative of line-of-sight binarity or activity are not apparent, and we conclude that the radial-velocity variations are genuinely due to the orbital motion of a low mass object.

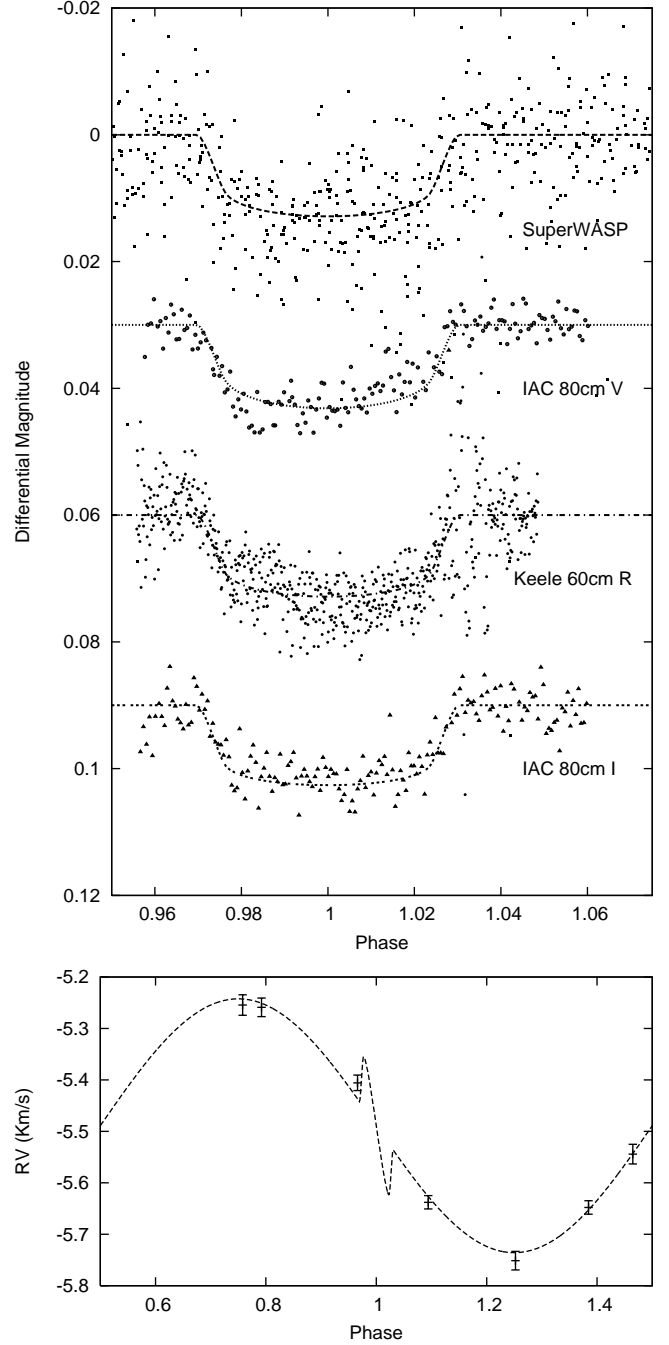


Figure 3. Simultaneous MCMC solution to combined SuperWASP-N, IAC80 V, I and Keele R photometry. The orbital solution is assumed to be circular. The lower panel is the MCMC solution to the radial velocity data. The model here also shows the Rossiter-McLaughlin effect which is predicted to be significant in this system given the hosts $v \sin i = 13.40$ km/s.

3.3 Adaptive Optics Imaging

We further investigated the scenario of a triple system comprising a bright single star and a faint, blended eclipsing-binary system by performing high-resolution H-band imaging with the near-infrared camera INGRID, fed by the adaptive-optics system NAOMI, on the 4.2-m William

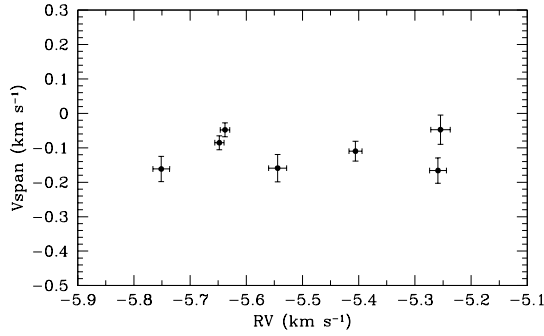


Figure 4. Analysis of line-bisectors in WASP-3 shows the bisector velocity (v_{span}) does not correlate with stellar radial-velocity. This demonstrates that the cross-correlation function remains symmetric, and that the radial-velocity variations are not likely to be caused by line-of-site binarity or stellar activity.

Herschel telescope. An image taken in natural seeing of 0.8 arcsecond with corrected FWHM of 0.2 arcsecond shows no evidence for resolved faint companions to WASP-3. Assuming an F7-8V spectral type ($M_v \sim 3.8$) for WASP-3 would imply a distance of ~ 220 pc, hence these observations constrain any potential associated eclipsing binary companion to lie within ~ 45 AU of the host.

4 DISCUSSION

In this study we have found WASP-3b to be a transiting gas-giant exoplanet with mass $1.76^{+0.08}_{-0.14} M_J$ and radius $1.31^{+0.07}_{-0.14} R_J$. Its host star, WASP-3, has a photospheric temperature of 6400 ± 100 K and $\log g = 4.25 \pm 0.05$, consistent with its F7-8V spectral type derived from 2MASS photometry. This places WASP-3b amongst the most massive of known transiting exoplanets (Figure 5). Given the hosts relatively large rotational velocity and the large radius of the planet we would expect a significant amplitude for Rossiter-McLaughlin effect (the model is included in Figure 3).

Sozzetti et al. (2007) demonstrate a correlation of planet radius with host mass for 14 confirmed transiting exoplanets, and a correlation of planet mass with orbital period for the same sample (first noted by Mazeh et al. (2005)). Figure 6 shows these relationships updated while in Figure 7 we also update the apparent correlation of surface gravity with orbital period noted by Southworth et al. (2007). Despite the additional objects the R_P v's M_* correlation remains weak (even ignoring the two most massive objects HD17156b and HD147506b). For both the M_P v's P and g v's P we contend that these relationships arise partly through observational selection and partly through the effects of the intense radiation fields that these planets are experiencing. We believe the absence of high gravity/mass bodies at longer periods is primarily a detection effect, while the absence of low gravity/mass planets at short period could indeed be caused by rapid evaporation.

The closeness of the orbit and the large radius and high effective temperature of the star combine to make WASP-3b one of the most strongly-irradiated, and hence one of the hottest of the known exoplanets, second only to OGLE-

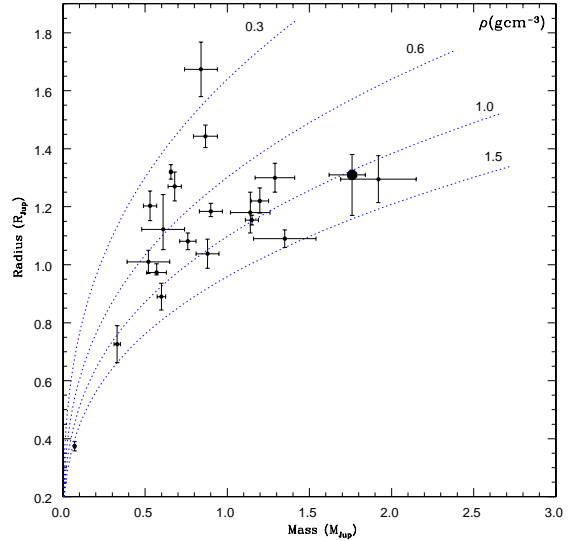


Figure 5. The known confirmed transiting exoplanets plotted in the Mass-Radius plane. Iso-density contours are plotted in cgs units. For clarity of scale we have not plotted HD17156 (mass $3.12 M_J$, radius $1.15 R_J$) or the extremely high density object HD147506b (mass $8.04 M_J$, radius $0.98 R_J$). WASP-3b is marked as a filled circle (data from <http://obswww.unige.ch/~pont/TRANSITS.htm> and references therein).

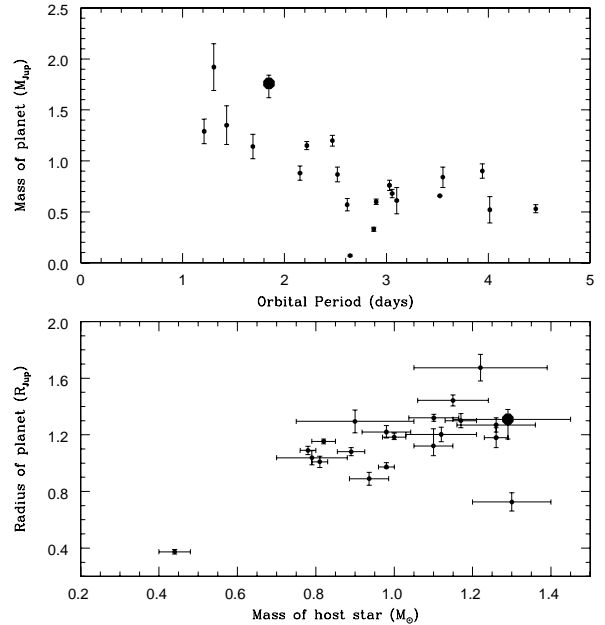


Figure 6. Modified version of Figure 5 from Sozzetti et al. (2007), incorporating a further seven newly discovered systems (data from <http://obswww.unige.ch/~pont/TRANSITS.htm> and references therein, but again excluding HD17156b and HD147506b). In each case WASP-3b is marked by the filled circle.

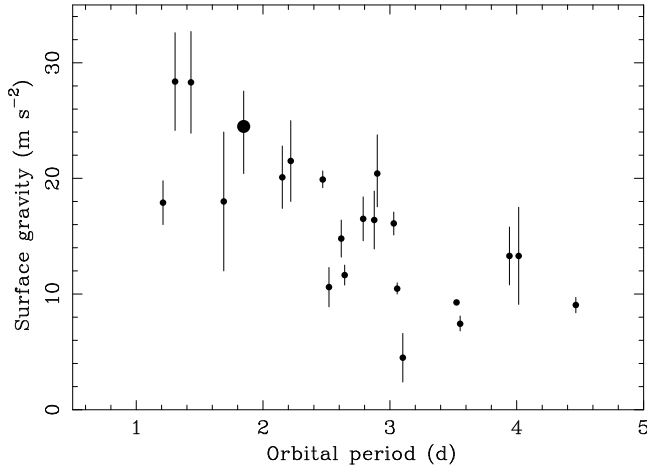


Figure 7. The correlation of planetary surface gravity with orbital period for the 22 shortest period transiting planets (updated version from Figure 2 from Southworth et al. (2007)).

TR-56b and comparable to OGLE-TR-132. This raises the possibility that the atmosphere may be hot enough for TiO and VO to remain in the gas phase above the temperature minimum, creating a hot, strongly-absorbing stratosphere (Fortney et al. 2006). This would give an anomalously high infrared brightness temperature, as Harrington et al. (2007) inferred from *SPITZER/IRAC* secondary-eclipse photometry of HD 149026b at $8\mu\text{m}$. Being much closer and brighter than any of the OGLE host stars, WASP-3b is thus an excellent candidate for future observational tests of the hot-stratosphere hypothesis.

ACKNOWLEDGMENTS

The WASP Consortium consists of astronomers primarily from the Universities of Cambridge (Wide Field Astronomy Unit), Keele, Leicester, The Open University, Queen's University Belfast and St Andrews, the Isaac Newton Group (La Palma), the Instituto de Astrofísica de Canarias (Tenerife) and the South African Astronomical Observatory. The SuperWASP-N and WASP-S Cameras were constructed and operated with funds made available from Consortium Universities and the UK's Science and Technology Facilities Council (formerly PPARC). We extend our thanks to the Director and staff of the Isaac Newton Group of Telescopes and the South African Astronomical Observatory for their support of SuperWASP-N and WASP-S operations, and the Director and staff of the Observatoire de Haute-Provence for their support of the SOPHIE spectrograph.

REFERENCES

Arras P., Bildsten L., 2006, *ApJ*, 650, 394
 Bakos G.A., Noyes R.W., Kovács G., Stanek K.Z., Sasselov D.D., Domsa I., 2004, *PASP*, 116, 266
 Berry R., Burnell J., 2005, *The handbook of astronomical image processing*, 2nd Edition, Richmond, VA (Willmann-Bell)

Blackwell D.E., Shallis M.J., 1977, *MNRAS* 180, 177
 Bouchy F., The Sophie Team, 2006, in Arnold L., Bouchy F., Moutou C., eds, Tenth Anniversary of 51 Peg-b: Status of and prospects for hot Jupiter studies, pp 319 – 325.
 Burke C.J., et al., 2007, *ApJ*, Submitted (arXiv:astro-ph 0705.0003)
 Burrows A., Hubeny I., Budaj J., Hubbard W.B., 2007, *ApJ*, 661, 502
 Collier Cameron A., et al., 2006, *MNRAS*, 373, 799
 Collier Cameron A., et al., 2007a, *MNRAS*, 375, 951
 Collier Cameron A., et al., 2007b, *MNRAS*, 380, 1230
 Christian D., et al., 2006, *MNRAS*, 372, 1117
 Charbonneau D., et al., 2000, *ApJ*, 529, 45L
 Claret A., 2000, *A&A*, 363, 1081
 Clarkson W., et al., 2007, *MNRAS*.tmp..824C
 Dunham E.W., Mandushev G.I., Taylor B.W., Oetiker B., 2004, *PASP*, 116, 1072
 Ford E.B., 2006, *ApJ*, 642, 505
 Fortney J.J., Saumon D., Marley M.S., Lodders K., Freedman R.S., 2006, *ApJ*, 642, 495
 Fortney J.J., Marley M.S., Barnes J.W., *ApJ*, 659, 1661
 Girardi L., Bressan A., Bertelli G., Chiosi C., 2000, *A&AS*, 141, 371
 Gregory P.C., 2007, *MNRAS*, 374, 1321
 Gray D.F., 1988, *Lectures on Spectral-line Analysis: F, G, and K Stars* (Arva, Ontario: Publisher)
 Gu P., Bodenheimer P.H., Lin D.N.C., 2004, *ApJ*, 608, 1076
 Guillot T., et al., 2006, *A&A*, 453, L21
 Harrington J., Luszcz S., Seager S., Deming D., Richardson L.J., 2007, *Nature*, 447, 691
 Henry G.W., Marcy G.W., Butler R.P., Vogt S.S., 2000, *ApJ*, 529, L41
 Holman M.J., et al., 2006, *ApJ*, 652, 1715
 Horne K.D., 2003, *Scientific Frontiers of Exoplanet Research*, ASP Conf. 294, 361, eds. Deming & Seager (San Francisco)
 Irwin M., Lewis J., 2001, *New Astronomy Reviews*, 45, 105
 Lister T., et al., 2007, *MNRAS*, 379, 647
 Mandel K., Agol E., 2002, *ApJ*, 580, L171
 Mayor M., Queloz D., 1995, *Nature* 378, 355
 Mazeh T., Zucker S., Pont F., 2005, *MNRAS*, 356, 955
 McCullough P.R. et al. 2006, *ApJ*, 648, 1228
 O'Donovan F.T., et al., 2006, *ApJ*, 644, 1237
 Piskunov, N. E., & Valenti, J. A. 2002, *A&A* 385, 1095
 Pollacco, D., et al., 2006, *ApJ*, 106, 1088
 Pont F., Zucker S., Queloz D., 2006, *MNRAS*, 373, 231
 Queloz D., et al., 2001, *A&A*, 379, 279
 Sato B., et al., 2005, *ApJ*, 633, 465
 Sestito P., Randich S., 2005, *A&A*, 442, 615
 Southworth J., Wheatley P.J., Sams G., 2007, *MNRAS*, 379, L11
 Sozzetti A., Torres G., Charbonneau D., Latham D.W., Holman M.J., Winn J.N., Laird J.B., O'Donovan F.T., 2007, preprint (arXiv:astro-ph 0704.2938v1)
 Street R.A., et al., 2007, *MNRAS*, 379, 816
 Stempels H.C., Collier Cameron A., Hebb L., Smalley B., Frandsen S., 2007, *MNRAS*, 379, 773
 Tegmark M., et al., 2004, *PhRvD*, 69, 103501
 Udalski A., et al., 2002, *Acta Astron.*, 52, 1
 Valenti J.A., Fischer D., 2005 *ApJS* 159, 141
 Valenti J.A., Piskunov N., 1996 *A&AS*, 118, 595

This paper has been typeset from a \TeX / \LaTeX file prepared by the author.